Article

Identifying Optimal Hot Forming Conditions for AA6010 Alloy by Means of Elevated Temperature Tensile Testing

Scott Taylor [1,*], Sisir Dhara [1], Carl Slater [1] and **Hiren Kotadia [1,2]**

1 Warwick Manufacturing Group, University of Warwick, Coventry CV4 7AL, UK
2 School of Engineering, Liverpool John Moores University, Liverpool L3 3AF, UK
* Correspondence: scott.taylor.1@warwick.ac.uk

Abstract: AA6010 in the F temper was investigated using a Gleeble 3800 test rig across a range of temperatures (350–550 °C) and strain rates (1×10^{-1} s^{-1} 1×10^{1} s^{-1}) to identify optimal forming conditions. Post-forming electron back-scattered diffraction analysis was conducted to identify the mechanisms responsible for the material formability. Optimal forming conditions were observed to be 500 °C and a strain rate of 1×10^{-1} s^{-1}, with clear evidence of dynamic recrystallisation observed, this being the dominant mechanism responsible for the increased formability. Peak yield strength of 335 MPa was achieved using a rapid aging treatment of 205 °C for one hour.

Keywords: aluminium; hot forming; Gleeble; HFQ; EBSD

1. Introduction

The current urgent need to reduce the impact of road vehicles on the environment is being approached from two sides: firstly, electrification of vehicles by replacing the more traditional polluting internal combustion engine (ICE); and, secondly, by improving the efficiency of ICE vehicles [1]. To counteract the increased weight of battery packs and motors in electric vehicles and to improve the efficiency of ICE vehicles, higher strength materials are required which allow for downgauging when compared to lower strength materials [2,3]. The 6000-series aluminium alloys offer an attractive solution to this problem, offering an extremely good strength to weight ratio, good processability, and, when combined with the correct forming process, high levels of formability [4].

Aluminium can easily replace steel material in applications such as automotive closures; there are many highly aluminium intensive vehicles on the market today, examples of early adopters of this technology being Audi with the A8 [5]. High strength aluminium's limited ductility at room temperature, however, requires the use of advanced forming processes to achieve sufficient elongations to produce more complex geometries for body-in-white structures such as B-pillars [6]. The use of elevated temperature forming processes such as superplastic forming (SPF), quick plastic forming (QPF), and hot form quench forming (HFQ) all take advantage of aluminium's increased ductility at elevated temperatures [7,8].

Hot forming of aluminium is now a widely employed process within the automotive field and with improvements in forming processes is moving from niche applications to more high-volume manufacturing. The 5000-, 6000- and 7000-series are all used in combination with hot forming to produce deep drawn parts of complex geometries [9–11]. Various studies have demonstrated the suitability of AA6082 in combination with the HFQ forming process to achieve deep drawn high strength parts with complex geometries [12]. Other alloys such as AA6061 and AA6111 have been shown to exhibit improved formability when combined with warm deep drawing [13,14]. AA6013 has also been demonstrated to be suitable within warm forming operations, and AA6010 is listed within a range of aluminium alloys suitable for hot forming in European patent EP3359699 [15,16]. These

alloys undergo solution heat treatment during the elevated temperature forming process; following quenching and subsequent aging treatments it is possible to produce complex geometries with high strength, able to replace steel structures.

The majority of published literature currently available on the subject focuses on AA6082 and its behaviour during HFQ forming; there are currently no available data on AA6010 under the same conditions [17–19]. This paper sets out to identify the optimum forming parameters for HFQ forming of AA6010 using a Gleeble 3800 testing machine and to identify a rapid post-forming heat treatment. Identifying the optimal forming parameters for the material and demonstrating its formability across a wide range of strain rates and temperatures will allow for better product and process design to meet industrial specifications. Identifying these optimum parameters will enable the forming of more complex part geometries where further weight savings can be achieved through part and fixture reduction; it has been demonstrated previously that SPF formed parts can reduce the overall weight of components and number of parts required in a wide range of applications [20].

2. Materials and Methods

Within this study AA6010 alloy nominally supplied in the F temper was investigated; the composition of the alloy as defined in the Aluminium Association Teal Sheets is given in Table 1 [21].

**Table 1.** AA6010 chemical composition in wt% [18].

Element	Al	Si	Fe	Cu	Mn	Mg	Cr	Zn	Ti
Wt%	Balance	0.8–1.2	0.5	0.15–0.6	0.2–0.8	0.6–1.0	0.1	0.25	0.1

Dog-bone shaped specimens were machined from 4 mm flat sheet using a Datron CNC machine (Datron Dynamics Inc., Milford, NH, USA), having a nominal gauge length of 15 mm and gauge width of 10 mm as shown in Figure 1. Previous studies have indicated that a shorter gauge length aids in achieving a homogenous temperature ± 5 °C throughout the specimen [17]. No further thermomechanical processing was carried out before testing.
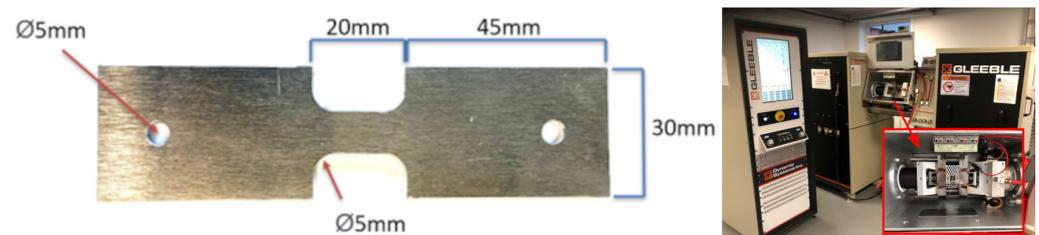
Figure 1. Sample geometry used for Gleeble thermomechanical processing, and Gleeble 3800 test machine (Gleeble, Poestenkill, NY, USA).

Hot tensile testing was carried out in a Gleeble 3800 in a similar methodology to previous studies on 2000- and 6000-series alloys [22,23]. K-type thermocouples were attached to the gauge length of the sample and a preload of 0.1 kN was applied to the sample. A typical thermal profile can be seen in Figure 2. The sample was heated to 565 °C at a rate of 7 °C/s where it was held for 5 min for solutionising; subsequently, the sample was cooled to the deformation temperature at 10 °C/s and held for 10 s, and then deformed to failure before being quenched to room temperature. A matrix of deformation temperatures and strain rates was used, comprising deformation temperatures every 50 °C between 350 and 550 °C, at strain rates of 0.1, 1 and 10 s^{-1} with 3 repeats for each condition. Test parameters were selected to investigate the most industrially relevant conditions under which this material would potentially be formed.
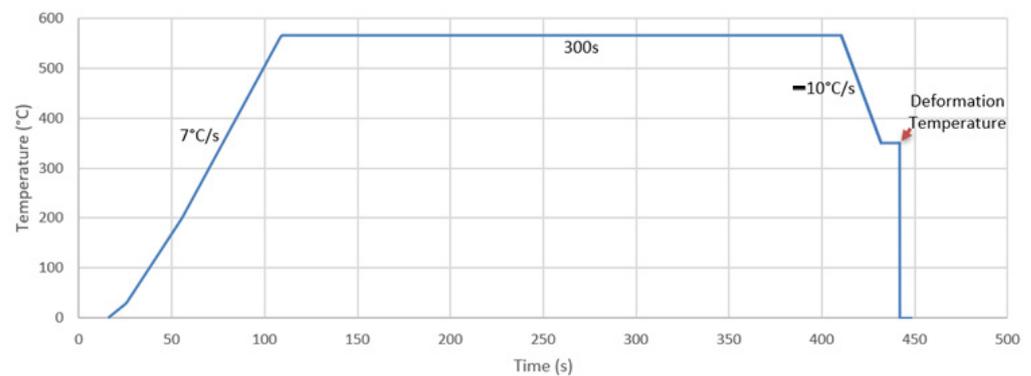
**Figure 2.** Thermal profile used during testing.

To identify the material's peak strength, it was subjected to the same thermal cycle as would be experienced during tensile tests but without any mechanical deformation being imparted; it then underwent an industrial aging treatment of 205 °C for one hour. Following heat treatments, the specimens were then subjected to room temperature tensile deformation to failure. The same thermal cycle as illustrated in Figure 2 but without any imparted deformation was used to prepare specimens for strength determination.

Microstructural analysis was conducted using a JEOL 7800F FEGSEM (JEOL Ltd., Tokyo, Japan) and an Oxford Instruments (Abingdon, UK) Symmetry electron back-scattered diffraction (EBSD) camera with Oxford Aztec software. An accelerating voltage of 20 keV was used across all scans, with a step size of 0.2 µm. Samples were prepared using a mechanical polishing regime modified from standard preparation techniques [24]; a final step of 30 min broad beam ion milling using a Hitachi IM4000 (Hitachi High-Technologies Corporation, Tokyo, Japan) operating at 4 kV was applied to achieve a high-quality surface finish. Post-processing of scans was conducted using Oxford Channel 5 software (Oxford Instruments, Abingdon, UK).

3. Results

3.1. Elevated Temperature Formability

Representative flow curves of the material tested across all temperatures and strain rates are illustrated in Figure 3, alongside the log stress-strain plot used to derive the material's 'm' value throughout testing. We observed reduced peak stresses in the material as the temperature increased with peak stresses of 95 MPa at 350 °C and 20 MPa at 550 °C as the material approached its melting temperature. A slight reduction in peak strain was observed from 500 °C to 550 °C; at this temperature further softening of the alloy led to promoted cavitation around secondary particles as shown in Figure 5 and led to premature failure. This demonstrates the alloy's ability to deform at elevated temperatures, a requirement for high strength aluminium alloys, but shows that increasing forming temperatures past 500 °C is not beneficial. The material exhibits a low 'm' value which is a material's strain rate sensitivity or its ability to resist localised necking; with a peak of around 0.18, this would indicate deformation controlled by dislocation creep as would be expected at such relatively high strain rates [25]. Previous studies have also reported low 'm' values for 6000-series alloys, which is beneficial as faster forming rates can be employed industrially without negatively impacting levels of formability [26].
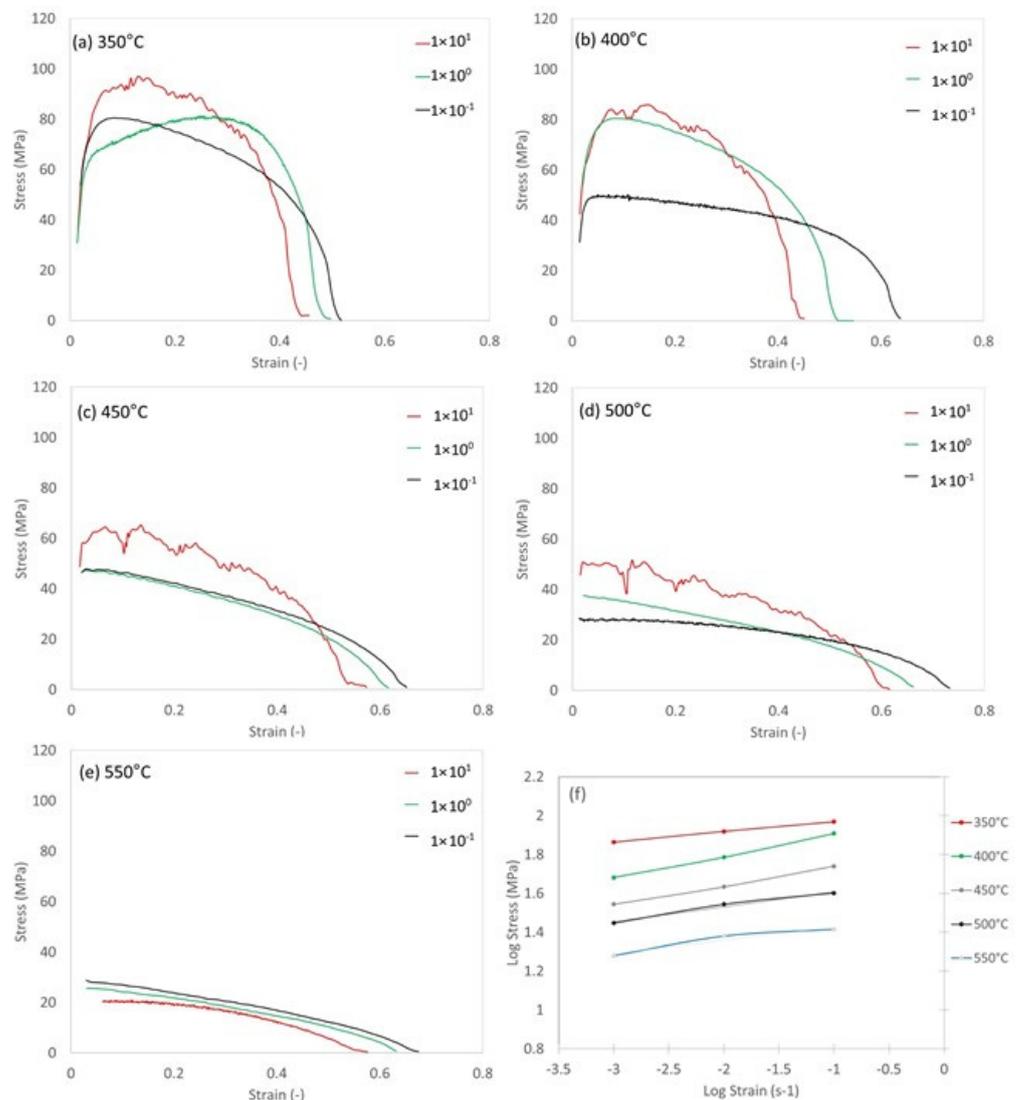
Figure 3. Stress vs. strain at (**a**) 350 °C, (**b**) 400 °C, (**c**) 450 °C, (**d**) 500 °C, and (**e**) 550 °C, (**f**) 'm' values of material across all temperatures at 0.1 strain.

To better illustrate the behaviour of the material across all conditions, forming processing maps illustrating strain to failure and peak stress are shown in Figure 4. Strain to failure increases due to the increased energy available at higher temperatures, which allows extra deformation mechanisms to become active within the microstructure. Figure 4 then better illustrates the reduction in peak strain at 550 °C compared to 500 °C due to excessive material softening. Similar reductions in strain to failure have been reported at lower temperatures in AA6082, indicating AA6010's ability to be formed at higher temperatures [23].

Aluminium alloys are strain rate sensitive during hot forming but as stated AA6010 is only slightly strain rate sensitive with an 'm' value ranging from 0.14–0.18; as such, we observe that for a given temperature the strain to failure decreases with increased strain rate but not by a significant amount. At 450 °C we see a decrease in strain to failure from 0.65 to 0.55 when the strain rate is increased from 1×10^{-1} s^{-1} to 1×10^{1} s^{-1}. Whilst this does not represent the material's optimal forming parameters, this region still offers industrially relevant levels of deformation.

Optimal forming conditions were observed to be 500 °C with a strain rate of 1×10^{-1} s^{-1}, giving a maximum strain to failure of around 0.7. It has been reported that dynamic recovery and dynamic recrystallization are the dominant deformation mechanisms with 6000-series

alloys at elevated temperatures. The strain rates during testing were greater than those where grain boundary sliding would occur, and so a combination of dislocation creep and dynamic recrystallization would have been responsible for the material's deformation.
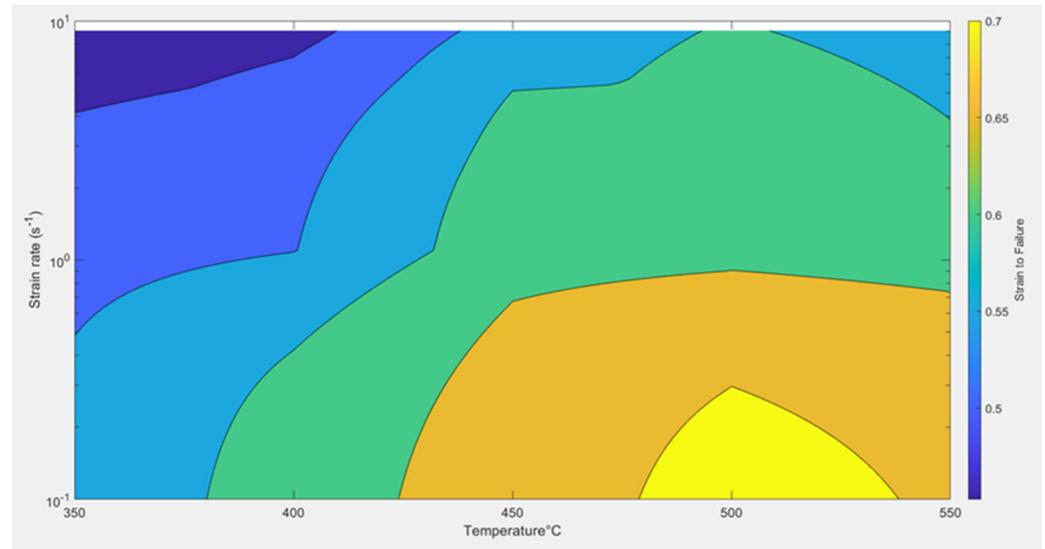
**Figure 4.** Strain to failure, strain rate, temperature forming parameter map.

3.2. EBSD Analysis of Deformed Specimens

EBSD maps from the failure region of samples deformed at 1×10^{-1} s^{-1} strain rate and three temperatures (350 °C, 400 °C and 500 °C) are shown in Figure 5a–c, respectively. Tearing failures can be observed within the 350 °C and 400 °C specimens with far more deformation and localised necking observed in the 500 °C specimen. With all specimens, tearing and void coalescence is evident in the presence of secondary particles which is more clearly shown in the band contrast image in Figure 5d where a clear tear in the bulk material is obvious as the grains have moved past the intermetallic.

Within the 350 °C and 400 °C specimens there are clear bands orientated in the direction of deformation, showing highly elongated grains; this is typical of deformation controlled by dislocation creep where grains elongate rather than rotate and move past each other. Within the 500 °C specimen the same 'bands' are visible; however, within these bands there are clearly new individual grains, showing the presence of dynamic recrystallization within the specimen during deformation. The presence of this extra deformation mechanism at the higher temperature is responsible for the increased peak strain at failure.

3.3. Post-Forming Heat Treatment

As with all 6000-series alloys, AA6010 is age-hardenable, which allows its use in a variety of high strength applications. To identify the suitability of the alloy within industrial applications, the strength of the material post-forming required investigation; this was done by applying a heat treatment cycle the same as that of the optimal forming conditions. Following solutionisation at 565 °C, specimens were then transferred to a furnace at 500 °C to replicate the optimum forming temperature, and then water quenched and then exposed to a rapid aging treatment of 205 °C for 1 h, to achieve a fine dispersion of Mg_2Si precipitates which inhibit dislocation movement. As shown in Figure 6 there is limited strain hardening of the material observed, indicating it has achieved its peak strength. Following artificial aging the material had an average 335 MPa yield strength with an average 11.5% axial strain.
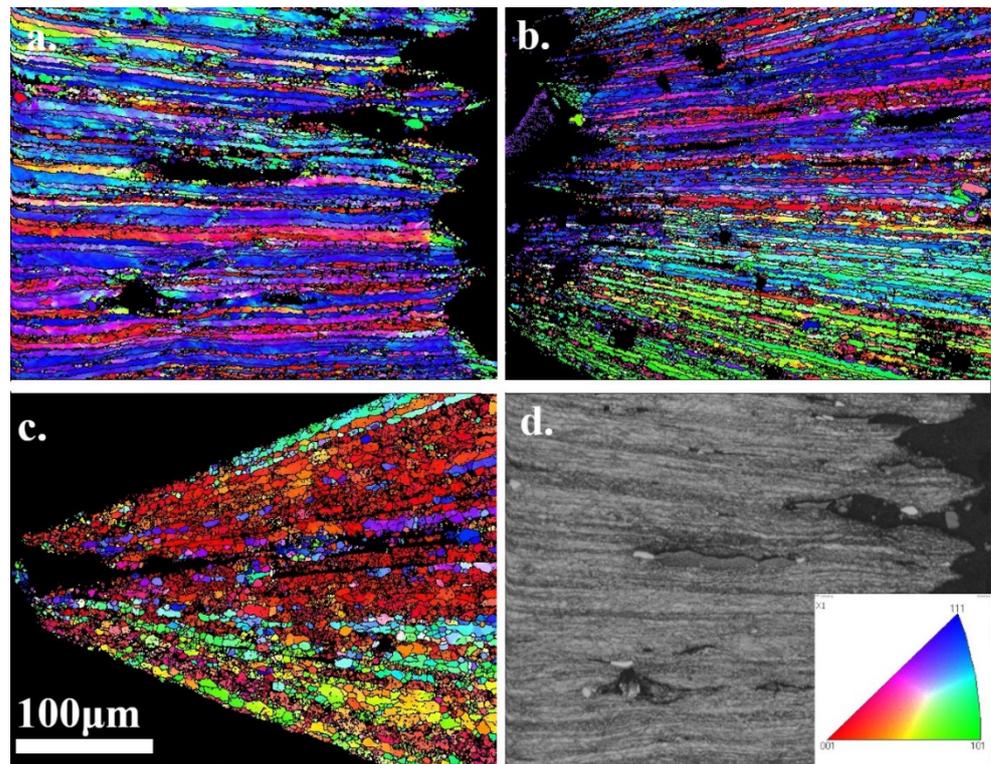
Figure 5. EBSD maps of failure region of specimens post-formed at 1×10^{-1} s^{-1} at (**a**) 350 °C, (**b**) 400 °C and (**c**) 500 °C and (**d**) band contrast image detailing tearing around intermetallics.
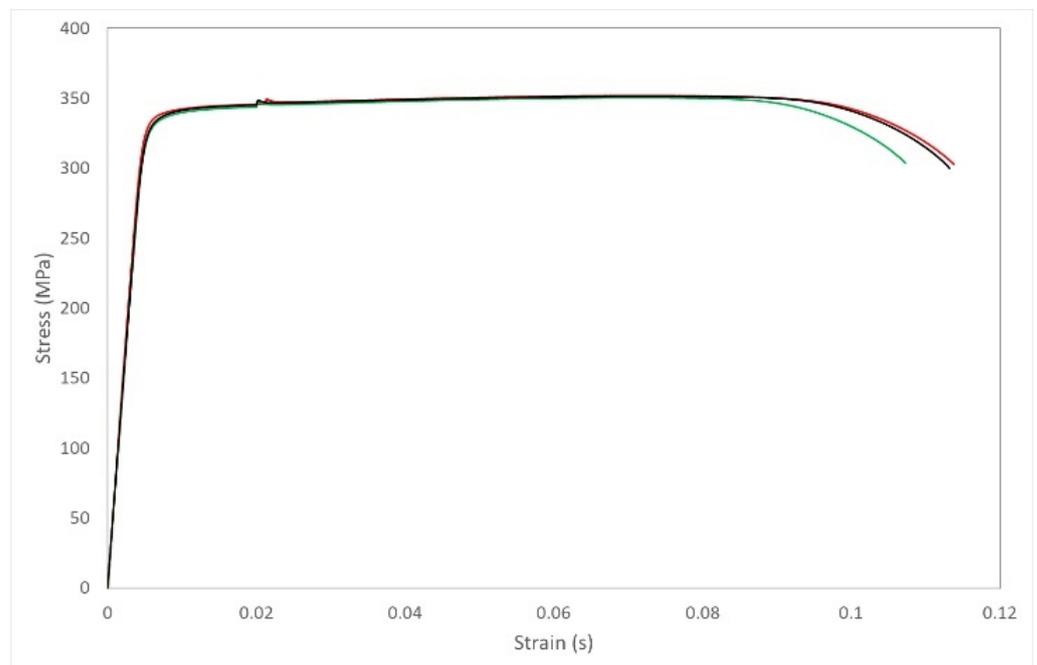
Figure 6. Flow curves of AA6010 following aging heat treatment.

4. Discussion

In this study the formability of AA6010 was investigated across a range of industrially applicable strain rates; optimal forming parameters were identified as 500 °C and 1×10^{-1} s^{-1} with peak strains of 0.7 achieved. Sub-optimal but still industrially relevant levels of formability were observed at lower temperatures and higher strain rates, with

a peak strain of 0.55 at 450 °C and 1×10^1 s^{-1}. Forming above 500 °C led to a decrease in peak strains with premature failures occurring due to excessive softening of the alloy around intermetallics.

The low 'm' value of the material combined with the evidence from EBSD results indicated that dislocation creep in combination with dynamic recrystallization are the dominant deformation mechanisms within the material. Coalescence of voids around intermetallics leading to tearing was responsible for failures within the material. The reduction of formability at 550 °C compared to 500 °C indicates that at the higher temperature, the rate of dynamic recrystallization is not sufficient to overcome the rate of development of voids due to excessive softening.

The ability to form the material at higher strain rates increases the potential industrial applications and shifts the use of the material towards higher volume manufacturing. To further investigate the suitability of the material within these applications, a rapid aging treatment was investigated; when combined with a preheating treatment to replicate optimal forming conditions, the material achieved a yield strength of 335 MPa. The material exhibited no evidence of strain hardening within this condition, indicating it had achieved peak strength, further demonstrating its suitability for automotive applications.

5. Conclusions

This paper set out to identify optimum forming parameters for AA6010 in an HFQ like forming process by means of elevated temperature tensile tests, and to demonstrate the material's suitability for use in industrial processes by assessing strength after a rapid aging treatment. From this work we conclude the following:

1. Optimal forming conditions for AA6010 in terms of peak ductility were established as 500 °C and 1×10^{-1} s^{-1} achieving a strain to failure of 0.7.
2. Industrially usable levels of deformation are achievable under sub-optimal conditions at 450 °C and 1×10^1 s^{-1} achieving a strain to failure of 0.55.
3. Dislocation creep and dynamic recrystallization are the dominant deformation mechanisms within AA6010 during HFQ like deformation.
4. Following rapid aging treatments the material can achieve a yield strength of 335 MPa.

Author Contributions: Conceptualization, S.T.; methodology, S.T. and C.S.; validation, S.T., S.D. and C.S.; formal analysis, S.T.; investigation, S.T., S.D., C.S. and H.K.; writing—original draft preparation, S.T.; writing—review and editing, S.T., S.D., C.S. and H.K.; project administration, S.T.; funding acquisition, S.T. and H.K. All authors have read and agreed to the published version of the manuscript.

Data Availability Statement: The data are not publicly available due to NDA agreements on commercially sensitive data.

Conflicts of Interest: The authors declare no conflict of interest.

References

1. Czerwinski, F. Current Trends in Automotive Lightweighting Strategies and Materials. *Materials* **2021**, *14*, 6631. [CrossRef]
2. Milovanoff, A.; Posen, I.D.; MacLean, H.L. Electrification of Light-Duty Vehicle Fleet Alone Will Not Meet Mitigation Targets. *Nat. Clim. Chang.* **2020**, *10*, 1102–1107. [CrossRef]
3. Miller, W.S.; Zhuang, L.; Bottema, J.; Wittebrood, A.J.; De Smet, P.; Haszler, A.; Vieregge, A. Recent Development in Aluminium Alloys for the Automotive Industry. *Mater. Sci. Eng. A* **2000**, *280*, 37–49. [CrossRef]
4. Long, R.S.; Boettcher, E.; Crawford, D. Current and Future Uses of Aluminum in the Automotive Industry. *JOM* **2017**, *69*, 2635–2639. [CrossRef]
5. Hirsch, J. Recent Development in Aluminium for Automotive Applications. *Trans. Nonferrous Met. Soc. China* **2014**, *24*, 1995–2002. [CrossRef]

6. Liu, Y.; Li, J.; Wang, L.; Wang, K.; Zhu, B.; Zhang, Y. Hot Stamping of a B-Pillar Reinforced Panel with 7075 Aluminum Alloy and the Feasibility Study of Short-Time Aging. *Front. Mater.* **2021**, *7*, 444. [CrossRef]
7. Zheng, K.; Politis, D.J.; Wang, L.; Lin, J. A Review on Forming Techniques for Manufacturing Lightweight Complex—Shaped Aluminium Panel Components. *Int. J. Light. Mater. Manuf.* **2018**, *1*, 55–80. [CrossRef]
8. Krajewski, P.E.; Schroth, J.G. Overview of Quick Plastic Forming Technology. *Mater. Sci. Forum* **2007**, *551–552*, 3–12. [CrossRef]
9. Dunwoody, B.J. The Production of Automotive Body Panels in 5083 SPF Aluminium Alloy. In *Proceedings of the Materials Science Forum*; Trans Tech Publications Ltd.: Bäch, Switzerland, 2001; Volume 357–359, pp. 59–64.
10. Meng, Q.; Wang, B.; Fu, L.; Zhou, J.; Lin, J. The Influence of Process Parameters during Hot Stamping of Aa6111 Aluminum Alloy Sheet. In *Proceedings of the Advanced Materials Research*; Trans Tech Publications: Bäch, Switzerland, 2012; Volume 572, pp. 255–260.
11. Rader, K.E.; Carter, J.T.; Hector, L.G.; Taleff, E.M. Plastic Deformation and Ductility of AA7075 and AA6013 at Warm Temperatures Suitable to Retrogression Forming. *Metall. Mater. Trans. A Phys. Metall. Mater. Sci.* **2021**, *52*, 4003–4017. [CrossRef]
12. El-Danaf, E.A.; Almajid, A.A.; Soliman, M.S. Hot Deformation of AA6082-T4 Aluminum Alloy. *J. Mater. Sci.* **2008**, *43*, 6324–6330. [CrossRef]
13. Liu, Y.; Zhu, Z.; Wang, Z.; Zhu, B.; Wang, Y.; Zhang, Y. Formability and Lubrication of a B-Pillar in Hot Stamping with 6061 and 7075 Aluminum Alloy Sheets. In *Proceedings of the Procedia Engineering*; Elsevier Ltd.: Amsterdam, The Netherlands, 2017; Volume 207, pp. 723–728.
14. Ma, W.Y.; Wang, B.Y.; Fu, L.; Zhou, J.; Huang, M.D. Influence of Process Parameters on Deep Drawing of AA6111 Aluminum Alloy at Elevated Temperatures. *J. Cent. South Univ.* **2015**, *22*, 1167–1174. [CrossRef]
15. Di Ciano, M.; DiCecco, S.; Esmaeili, S.; Wells, M.A.; Worswick, M.J. Coarsening of AA6013-T6 Precipitates during Sheet Warm Forming Applications. *J. Mater. Eng. Perform.* **2018**, *27*, 939–947. [CrossRef]
16. EPO—European Publication Server. Available online: https://data.epo.org/publication-server/document?iDocId=6324311&iFormat=0 (accessed on 3 March 2022).
17. Li, N.; Shao, Z.; Lin, J.; Dean, T.A. Investigation of Uniaxial Tensile Properties of AA6082 under HFQ®Conditions. *Key Eng. Mater.* **2016**, *716*, 337–344. [CrossRef]
18. Mohamed, M.S.; Foster, A.D.; Lin, J.; Balint, D.S.; Dean, T.A. Investigation of Deformation and Failure Features in Hot Stamping of AA6082: Experimentation and Modelling. *Int. J. Mach. Tools Manuf.* **2012**, *53*, 27–38. [CrossRef]
19. Liu, X.; Fakir, O.E.; Meng, L.; Sun, X.; Li, X.; Wang, L.L. Effects of Lubricant on the IHTC during the Hot Stamping of AA6082 Aluminium Alloy: Experimental and Modelling Studies. *J. Mater. Process. Technol.* **2018**, *255*, 175–183. [CrossRef]
20. Barnes, A.J. Industrial Applications of Superplastic Forming: Trends and Prospects. In Proceedings of the Materials Science Forum; Trans Tech Publications Ltd.: Bäch, Switzerland, 2001; Volume 357–359, pp. 3–16.
21. The Aluminum Association, Teal Seets. Available online: https://www.aluminum.org/sites/default/files/2021-10/Teal%20Sheet.pdf (accessed on 3 March 2022).
22. Jia, X.D.; Wang, Y.N.; Zhou, Y.; Cao, M.Y. The Study on Forming Property at High Temperature and Processing Map of 2219 Aluminum Alloy. *Metals* **2021**, *11*, 77. [CrossRef]
23. Wang, P.L.; Jiang, H.T.; Zhang, R.J.; Huang, S.Y. Study of Hot Deformation Behavior of 6082 Aluminum Alloy. In *Proceedings of the Materials Science Forum*; Trans Tech Publications Ltd.: Bäch, Switzerland, 2017; Volume 877, pp. 340–346.
24. Taylor, S.; Kotadia, H.R. Microstructural Evolution of 316L Austenitic Stainless Steel during In-Situ Biaxial Deformation and Annealing. *Mater. Charact.* **2020**, *163*, 110288. [CrossRef]
25. Sherby, O.D.; Wadsworth, J. Superplasticity-Recent Advances and Future Directions. *Prog. Mater. Sci.* **1989**, *33*, 169–221. [CrossRef]
26. Chen, X.; Peng, Y.; Peng, S.; Yao, S.; Chen, C.; Xu, P. Flow and Fracture Behavior of Aluminum Alloy 6082-T6 at Different Tensile Strain Rates and Triaxialities. *PLoS ONE* **2017**, *12*, e0181983. [CrossRef] [PubMed]